

## DISCOVERY OF A RADIO SUPERNOVA REMNANT AND NON-THERMAL X-RAYS COINCIDENT WITH THE TEV SOURCE HESS J1813–178

C. L. BROGAN<sup>1</sup>, B. M. GAENSLER<sup>2</sup>, J. D. GELFAND<sup>2</sup>, J. S. LAZENDIC<sup>3</sup>, T. J. LAZIO<sup>4</sup>, N. E. KASSIM<sup>4</sup>, N. M. MCCLURE-GRIFFITHS<sup>5</sup>

*Draft version November 6, 2018*

### ABSTRACT

We present the discovery of non-thermal radio and X-ray emission positionally coincident with the TeV  $\gamma$ -ray source HESS J1813–178. We demonstrate that the non-thermal radio emission is due to a young shell-type supernova remnant (SNR) G12.8–0.0, and constrain its distance to be greater than 4 kpc. The X-ray emission is primarily non-thermal and is consistent with either an SNR shell or unidentified pulsar/pulsar wind nebula origin; pulsed emission is not detected in archival *ASCA* data. A simple synchrotron+inverse Compton model for the broadband emission assuming that all of the emission arises from the SNR shell implies maximum energies of  $(30–450)(B/10\mu\text{G})^{-0.5}$  TeV. Further observations are needed to confirm that the broadband emission has a common origin and better constrain the X-ray spectrum.

*Subject headings:* acceleration of particles – supernova remnants – radio:ISM – Xrays:ISM – ISM: individual (G12.8-0.0, HESS J1813-178)

### 1. INTRODUCTION

Based on theoretical arguments, it has become widely accepted that a significant fraction of Galactic cosmic rays with energies up to the “knee” in the cosmic ray spectrum at  $\sim 10^{15}$  eV are generated in shell type supernova remnants (SNRs) (e.g. Blandford & Eichler 1987). While the detection of non-thermal X-rays from the shells of several SNRs provides evidence that SNR shocks are efficient accelerators of  $\lesssim 10^{13}$  eV electrons (see e.g. Reynolds 1996), direct evidence is still lacking that (1) SNRs can accelerate particles all the way to  $10^{15}$  eV, and (2) SNRs efficiently accelerate protons and heavy nuclei as well as electrons (see Pohl 2001, for a review). Powerful constraints on shock acceleration in SNRs can come from the detection of TeV  $\gamma$ -rays. However, these high energy photons can be produced by a variety of mechanisms, including inverse Compton (IC) emission from energetic electrons, and pion decay produced by the collision of energetic protons with surrounding dense gas. Additionally, pulsars, pulsar wind nebulae (PWNe), microquasars, and massive stars, have also been suggested as TeV counterparts, so it is unclear whether SNRs are in fact the primary source of cosmic rays  $\lesssim 10^{15}$  eV.

Currently only two convincing shell SNR/TeV associations are known (SNRs G347.3–0.5 and G266.2–1.2; Aharonian et al. 2004, 2005a), and observations do not yet unambiguously distinguish between hadronic and leptonic acceleration (Lazendic et al. 2004; Malkov, Diamond, & Sagdeev 2005). However, with the advent of new sensitive Čerenkov imaging telescopes, there are bright prospects for discovering additional TeV sources. Indeed, Aharonian et al. (2005b) recently reported the discovery of eight new TeV  $\gamma$ -ray sources in the inner Galactic

plane ( $\ell = \pm 30^\circ$ ) using the High Energy Stereoscopic System (HESS). Of the eight new TeV sources, six are listed in Aharonian et al. (2005b) as being in close proximity to either an SNR, pulsar, or *EGRET* source (in some cases all three). However, these authors were unable to identify any plausible counterparts to two of the new TeV sources and suggest that they may represent a new class of “dark” nucleonic particle accelerators.

In this *Letter* we present evidence that one of the two “dark” TeV sources, HESS J1813–178, is positionally coincident with a previously unidentified young radio and X-ray SNR, G12.8–0.0. A simple model for the broadband emission is also presented.

### 2. DATA AND RESULTS

#### 2.1. The Radio Source G12.82–0.02

The radio source G12.82–0.02 was discovered in a new low frequency Very Large Array (VLA) 90cm survey incorporating B+C+D configuration data (Brogan et al. 2005). The previously unidentified radio source has a shell morphology with a diameter of  $\sim 2.5'$ . Analysis of archival VLA C+D configuration 20cm data has confirmed this discovery, and indicates that the radio emission is non-thermal. G12.82–0.02 has integrated radio flux densities at 20 and 90 cm of  $0.65 \pm 0.1$  and  $1.2 \pm 0.08$  Jy, respectively. Figure 1a shows the 90cm image while Figure 1b shows a 3-color image of the region using 90cm, 20cm, and 8  $\mu\text{m}$  *Spitzer Space Telescope* GLIMPSE data (Benjamin et al. 2003). It is notable that no distinct (non-diffuse) dust emission is coincident with G12.82–0.02, confirming its non-thermal nature. HESS J1813–178 (positional uncertainty  $1'–2'$ ) is coincident with the radio shell (see Fig. 1a) and its size of  $\sim 3'$  is in excellent agreement with that of G12.82–0.02. No structure is evident in the published  $3'$  resolution HESS image (Aharonian et al. 2005b). The radio and TeV sources are located  $\sim 8'$  from the H II region complex W33 (see Fig. 1a,b, §3.1).

Though not previously recognized as a distinct source, G12.82–0.02 is evident as a faint unresolved extension to W33 in the Nobeyama 3cm, Parkes 6cm, and Bonn 11cm surveys, with resolutions ranging from  $3'$  to  $4.3'$  (Haynes et al. 1978; Handa et al. 1987; Reich et al. 1990). The radio spectrum of G12.82–0.02 (including the 20 and 90cm VLA

arXiv:astro-ph/0505145v2 13 Jul 2005

<sup>1</sup> Institute for Astronomy, 640 North A'ohoku Place, Hilo, HI 96720; cbrogan@ifa.hawaii.edu.

<sup>2</sup> Harvard-Smithsonian Center for Astrophysics, 60 Garden Street, Cambridge, MA 02138

<sup>3</sup> MIT Kavli Institute for Astrophysics and Space Research, Cambridge MA 02319

<sup>4</sup> Remote Sensing Division, Naval Research Laboratory, Washington DC 20375-5351

<sup>5</sup> Australia Telescope National Facility, CSIRO, P.O. Box 76, Epping, NSW 1710, Australia

data, 4m VLA B+C+D configuration data from Brogan et al. (2004), and the single dish data) is shown in Figure 1c. The rms noise in the 20 and 90cm images are 5 and 2.5 mJy beam<sup>-1</sup>, respectively, and the flux density uncertainty is (# independent beams)<sup>0.5</sup> × 3σ. G12.82–0.02 is not detected at 4m; the flux density shown in Figure 1c is a 5σ upper limit (also see §3.1). To account for the extra uncertainty due to confusion with W33, 6σ was used for the single dish uncertainties. The spectral index using these data (excluding the 4m non-detection) and a weighted least squares fit is  $-0.48 \pm 0.03$  (where  $S_\nu \propto \nu^\alpha$ ), similar to that of other small shell type SNRs (i.e. G349.7+0.2 and W49B) without central pulsars (Green 2004).

Assuming  $\alpha = -0.48$ , the 1 GHz surface brightness of G12.82–0.02 is  $\Sigma_{1\text{GHz}} \sim 3.3 \times 10^{-20} \text{ W m}^{-2} \text{ Hz sr}^{-1}$ , and the radio luminosity from  $10^7 - 10^{11} \text{ Hz}$  is  $\sim 3.6(d/d_4)^2 \times 10^{32} \text{ ergs s}^{-1}$  ( $d$  is the distance and  $d_4 = 4 \text{ kpc}$ ; see §3.1). The radio morphology, radio spectrum, and lack of coincident mid-infrared emission (Fig. 1) provide convincing evidence that G12.82–0.02 is a previously unidentified shell type SNR; henceforth designated SNR G12.8–0.0.

### 2.2. The X-ray Source AX J1813–178

Analysis of a pointed 100 ks archival ASCA observation toward this region (taken 1997 September) reveals a source, hereafter AX J1813–178, spatially coincident with both SNR G12.8–0.0 and HESS J1813–178 (see Figure 2). AX J1813–178 is detected by both the SIS and GIS ASCA instruments, although the emission is contaminated in the GIS detectors by the bright X-ray binary GX 13+1  $\sim 40'$  to the NE. Thus, we have confined our spectral and imaging analysis to the SIS data with a combined (screened) exposure time of  $\sim 64 \text{ ks}$ . The X-ray source appears to be either unresolved or slightly extended (Fig 2). The X-ray peak nominally lies interior to the radio shell, but since the ASCA pointing uncertainty can be as large as  $1'$  (Gotthelf et al. 2000), the ASCA image does not distinguish between X-rays originating from the center (i.e. a compact object) or the shell of the SNR.

The X-ray spectrum is quite hard, with emission extending to 10 keV and a strong cut-off below 2 keV; no lines are evident (inset Fig. 2). Thus it is clear that the emission is predominately non-thermal. The background-corrected SIS data (extracted from a  $3'$  source region) consisting of  $\approx 2000$  counts in the energy range 0.5–10 keV were jointly fit to several absorbed spectral models including a power-law, and 2-component combinations of a power-law plus a (1) Raymond-Smith (RS) thermal plasma (with and without the abundances frozen at solar), (2) blackbody, and (3) Bremsstrahlung component. The data quality are such that all of these models give reasonable fits (reduced  $\chi^2 \sim 1$ ).

Statistically, a power-law plus RS model gives the best fit (RS  $kT \sim 0.22 \pm 0.1 \text{ keV}$ ) but the improvement is only  $4\sigma$  compared to a power-law alone; the emission measure of the RS component cannot be constrained. This result suggests that higher quality X-ray data are needed to determine the thermal contribution to the X-ray emission (see also Ubertini et al. 2005). None of the two-component fits yield a significantly different absorbing column or photon index compared to the power law fit alone:  $N_H = (10.8_{+2.3}^{1.9} \times 10^{22} \text{ cm}^{-2})$  and  $\Gamma = 1.83_{+0.42}^{-0.37}$ . The unabsorbed flux and luminosity of AX J1813–178 from 2–10 keV are  $\sim 7.0 \times 10^{-12} \text{ ergs cm}^{-2} \text{ s}^{-1}$  and  $1.7(d/d_4)^2 \times 10^{34} \text{ ergs s}^{-1}$ , respectively. These parameters are consistent with AX J1813–178 being either a pul-

sar/PWN or one of a small number of primarily non-thermal X-ray SNRs such as G266.2–1.2 and G347.3–0.5.

## 3. DISCUSSION

### 3.1. Distance Constraints

As mentioned previously, SNR G12.8–0.0 lies near the line of sight of the W33 H II region/star formation complex. The radio recombination lines, molecular lines (including masers), and H I gas associated with W33 arise from LSR velocity components at  $\sim +30$  and  $\sim +50 \text{ km s}^{-1}$  (e.g. Sato 1977; Bieging et al. 1978; Gardner et al. 1983). No H I absorption features are evident toward W33 beyond  $\sim +55 \text{ km s}^{-1}$  (Radhakrishnan et al. 1972). Since the tangent point velocity is  $\sim +170 \text{ km s}^{-1}$  in this direction (assumes Galactic center distance 8.5 kpc and Fich et al. 1989, rotation curve), W33 must lie at about the  $+55 \text{ km s}^{-1}$  near distance of  $\sim 4.3 \text{ kpc}$ . Similar to W33, H I absorption spectra from the Southern Galactic Plane Survey (resolution  $1'$ , see McClure-Griffiths et al. 2005) toward G12.8–0.0 show absorption to, but not beyond  $\sim +55 \text{ km s}^{-1}$ , although the signal-to-noise is low. Thus, the distance to G12.8–0.0 is likely to be  $\gtrsim 4 \text{ kpc}$ .

Based on the derived radio spectral index ( $-0.48$ ) the expected 4m flux density is  $\sim 2.7 \text{ Jy}$ , suggesting that SNR G12.8–0.0 should be readily detectable, yet it is not (Fig. 1c, §2.1). This discrepancy could be due to the close proximity of W33 if G12.8–0.0 lies immersed in or behind the H II region due to free-free absorption (see e.g. Kassim 1989). In interferometric low frequency images ( $\nu \lesssim 100 \text{ MHz}$ ) H II regions can appear in absorption against the resolved out diffuse Galactic plane synchrotron emission due to free-free absorption. W33 is coincident with such a 4m absorption 'hole'; its morphology is similar to the diffuse 90cm and  $8 \mu\text{m}$  emission (Fig. 1b) and extends as far west as G12.8–0.0. Thus, free-free absorption is the most natural explanation for the non-detection of G12.8–0.0 at 4m, and confirms the H I result that the SNR must lie at the distance of or behind W33.

The high column density derived from the ASCA data,  $N_H \sim 10^{23} \text{ cm}^{-2}$ , also suggests that SNR G12.8–0.0 lies behind W33. Along nearby lines of sight, the integrated Galactic H I column density is only  $\sim 2 \times 10^{22} \text{ cm}^{-2}$  (Dickey & Lockman 1990), suggesting that a significant discrete source of absorption must be in the foreground to the SNR. CO data (Dame et al. 2001) indicate that dense gas in the distance range 0–4 kpc (much of which is associated with W33) contributes a hydrogen column density  $\sim 8 \times 10^{22} \text{ cm}^{-2}$ , and can thus account for much of the X-ray absorption. This further argues for a distance of 4 kpc or greater for SNR G12.8–0.0; we adopt a fiducial minimum distance of 4 kpc ( $d_4$ ) for the remaining discussion.

### 3.2. The Probable Youth of SNR G12.8–0.0

The small angular size of SNR G12.8–0.0 ( $2.5'$ ) suggests that it is quite young; certainly the high extinction toward this region would have prevented its detection optically. The radius of SNR G12.8–0.0 is  $1.5(d/d_4) \text{ pc}$ . If the SNR is still freely expanding at a speed  $v_s$  its age is  $\sim 285(d/d_4) (v_s/v_5)^{-1} \text{ years}$  ( $v_5 = 5,000 \text{ km s}^{-1}$ ). Shock speeds of  $v_s = 5,000 \text{ km s}^{-1}$  are expected from SNRs with X-ray synchrotron emission (e.g. Aharonian & Atoyan 1999). If the distance is 4–10 kpc, use of the free-expansion age is justified since the swept up mass would still be a small fraction of the ejected mass. At greater distances the SNR is likely to have entered

the Sedov-Taylor phase. For example, at 20 kpc, the swept up mass is  $\sim 50 M_{\odot}$  (assuming an ambient density  $n_o = 1 \text{ cm}^{-3}$  and 10% helium abundance) and the Sedov-Taylor age is  $2,520(n_o)^{0.5}(E/E_{51})^{-0.5}$  years (where  $E$  is the kinetic energy and  $E_{51} = 10^{51}$  ergs). Thus, independent of distance, if G12.8–0.0 is expanding into a typical density medium it is very young with representative age estimates in the range 285–2,500 years. Excluding G12.8–0.0, only six shell type Galactic SNRs with diameters  $\lesssim 3'$  are currently known, undoubtedly due to observational selection effects since many more are expected (Green 2004). Our discovery highlights the effectiveness of high resolution and sensitivity low radio frequency surveys in finding young Galactic SNRs.

### 3.3. X-ray and TeV Emission from a Young Pulsar?

Although there is excellent positional agreement between the radio, X-ray, and TeV emission (Fig. 2), it is currently unclear whether all these components originate from the SNR shell or if there is an as yet unidentified associated pulsar or PWN. No central radio nebula or point source is detected at our current spatial resolution and sensitivity, and there are no known radio pulsars within  $16'$  of the SNR (Manchester et al. 2005). This field has been searched for pulsars as part of the Parkes multi-beam pulsar survey, to a limiting 1.4 GHz flux density of 0.2 mJy (Manchester et al. 2001), corresponding to a pseudo-luminosity of  $\sim 3(d/d_4)^2$  mJy kpc<sup>2</sup>. Recent deep pulsar searches toward SNRs have been able to either detect or place upper limits of  $\sim 1$  mJy kpc<sup>2</sup> on the 1.4 GHz pseudo-luminosity of central pulsars (e.g. Camilo et al. 2002). Thus, the Parkes multi-beam survey is reasonably constraining, but a deeper search is needed.

The X-ray luminosity and photon index inferred in §2.2 for AX J1813–178 are typical of young pulsars and their associated PWN (e.g. Possenti et al. 2002). In order to search for X-ray pulsations from AX J1813–178 we conducted a  $Z_n^2$  search (see Buccheri et al. 1983) on the barycenter-corrected ASCA high-bit mode GIS data (with 20 ks of data). No pulsed signal was detected using 585 counts between 4–8 keV. For periods between 125 ms and 1000 s, we find an upper limit on the pulsed fraction of 38% (19%) for a sinusoidal (sharply peaked) pulse profile. Since most young pulsars rotate with periods below this range, and the pulsed signal may be a small fraction ( $< 10\%$ ) of the total pulsar plus PWN X-ray flux, the lack of pulsations is not very constraining. Deeper X-ray and radio observations of this source are needed to confirm or rule out a pulsar/PWN interpretation for AX J1813–178.

### 3.4. X-ray and TeV Emission from the SNR Shell?

The radio (SNR shell) and X-ray (origin uncertain) data fit smoothly onto a single power-law+rolloff spectrum, unlike the typical behavior of PWN, suggesting they have a common origin (Figure 3). Assuming that the radio, X-ray, and TeV emission originate from the SNR shell, we have modeled the flux expected from synchrotron+IC mechanisms using a

power law energy distribution modified by an exponential cut-off  $dN/dE \approx E^{-\sigma} \exp[-(E/E_{max})]$  (where  $\sigma$  is the index of the electron distribution, and  $E_{max}$  is the maximum energy of accelerated particles, see Lazendic et al. 2004). Since the X-ray absorption column (and hence X-ray spectral index) is not well constrained by the ASCA data, two variations of this model are shown in Figure 3, one using the best fit X-ray  $N_H$  (red) and the other using the  $1\sigma$  lower limit to  $N_H$  (blue). Together these models encompass the likely range of parameter space. We have assumed a 15% filling factor for the magnetic field in the IC emitting region in order to obtain the best agreement with the HESS data for the ‘blue’ model; larger values yield lower IC components. The fitted broad-band electron spectral indices are  $\sigma = 2.3$  (red) and  $\sigma = 2.0$  (blue) – the former is consistent with the best-fit photon index for the ASCA spectrum, while the latter is more consistent with the radio spectral index.

The roll-off frequencies ( $\nu_{ro}$ ) derived from the synchrotron spectra are  $3.3 \times 10^{19}$  Hz (red) and  $1.3 \times 10^{17}$  Hz (blue). The maximum energy is related to  $\nu_{ro}$  and the magnetic field strength  $B$  by  $\nu_{ro} \sim 1.6 \times 10^{16} (B/10 \mu\text{G}) (E_{max}/10 \text{ TeV})^2$  Hz, so that  $E_{max} = 450 (B/10 \mu\text{G})^{-0.5}$  TeV (red) and  $E_{max} = 30 (B/10 \mu\text{G})^{-0.5}$  TeV (blue). Thus, unless the magnetic field strength is much stronger than  $10 \mu\text{G}$  (see for example Völk et al. 2005),  $E_{max}$  for this source is potentially rather high (e.g. Reynolds & Keohane 1999). Additionally, for much of the parameter space range, the IC emission from CMB scattering alone is insufficient to account for the HESS data; the discrepancy is larger for larger values of  $B$ . It is possible a more sophisticated IC model incorporating scattering off starlight (Aharonian et al. 2005c) would better accommodate the HESS data. Indeed, Helfand et al. (2005) find this to be the case assuming the SNR lies at the distance of W33, though currently it is only constrained to be at or greater than this distance. It is also possible that the TeV emission arises from the acceleration of nuclei and subsequent pion decay instead of IC if the SNR is embedded in a sufficiently dense ambient medium (e.g. Uchiyama et al. 2005). Detection of resolved X-ray and TeV emission from the SNR shell would strengthen our suggestions that the radio, X-ray, and TeV emission have the same origin. Higher sensitivity X-ray data will also be crucial to better constrain the properties of the broadband emission.

Basic research in radio astronomy at the Naval Research Laboratory is supported by the Office of Naval Research. The VLA is operated by the National Radio Astronomy Observatory – a facility of the National Science Foundation operated under cooperative agreement by Associated Universities, Inc. This research made use of HEASARC, provided by NASA’s Goddard Space Flight Center. We thank L. Rickard, D. Ellison, and S. Reynolds for helpful discussions.

## REFERENCES

- Aharonian, F., et al. 2005a, A&A, in press, astro-ph/0505380  
 Aharonian, F., et al. 2005b, Science, 307, 1938  
 Aharonian, F., et al. 2005c, A&A, 432, L25  
 Aharonian, F. A., et al. 2004, Nature, 432, 75  
 Aharonian, F. A., & Atoyan, A. M. 1999, A&A, 351, 330  
 Benjamin, R. A., et al. 2003, PASP, 115, 953  
 Biegging, J. H., Pankonin, V., & Smith, L. F. 1978, A&A, 64, 341  
 Blandford, R., & Eichler, D. 1987, Phys. Rep., 154, 1  
 Brogan, C. L., et al. 2004, AJ, 127, 355  
 Brogan, C. L., Gelfand, J. D., Gaensler, B. M., Kassim, N. E., & Lazio, T. J., 2005, in prep.  
 Buccheri, R., et al. 1983, A&A, 128, 245  
 Camilo, F., Manchester, R. N., Gaensler, B. M., & Lorimer, D. R. 2002, ApJ, 579, L25  
 Dame, T. M., Hartmann, D., & Thaddeus, P. 2001, ApJ, 547, 792  
 Dickey, J. M., & Lockman, F. J. 1990, ARA&A, 28, 215

Fich, M., Blitz, L., & Stark, A. A. 1989, *ApJ*, 342, 272  
 Gardner, F. F., Whiteoak, J. B., & Otrupcek, R. E. 1983, *Proceedings of the Astronomical Society of Australia*, 5, 221  
 Green, D. A. 2004, *Bull. Astro. Soc. India*, 32, 335  
 Gotthelf, E. V., Ueda, Y., Fujimoto, R., Kii, T., & Yamaoka, K. 2000, *ApJ*, 543, 417  
 Helfand, D. J., Becker, R. H., & White, R. L. 2005, *astro-ph/0505392*  
 Handa, T., Sofue, Y., Nakai, N., Hirabayashi, H., & Inoue, M. 1987, *PASJ*, 39, 709  
 Haynes, R. F., Caswell, J. L., & Simons, L. W. J. 1978, *Australian Journal of Physics Astrophysical Supplement*, 45, 1  
 Kassim, N. E. 1989, *ApJ*, 347, 915  
 Lazendic, J. S., Slane, P. O., Gaensler, B. M., Reynolds, S. P., Plucinsky, P. P., & Hughes, J. P. 2004, *ApJ*, 602, 271  
 Malkov, M. A., Diamond, P. H., & Sagdeev, R. Z. 2005, *ApJ*, 624, L37  
 Manchester, R. N., et al. 2001, *MNRAS*, 328, 17  
 Manchester, R. N., Hobbs, G. B., Teoh, A., & Hobbs, M. 2005, *AJ*, 129, 1993

McClure-Griffiths, et. al. 2005, *ApJS*, in press, *astro-ph/0503134*  
 Pohl, M. 2001, “27th International Cosmic Ray Conference” ed. Schlickeiser, R., Copernicus Group, *astro-ph/0111552*  
 Possenti, A., Cerutti, R., Colpi, M., & Mereghetti, S. 2002, *A&A*, 387, 993  
 Radhakrishnan, V., Goss, W. M., Murray, J. D., & Brooks, J. W. 1972, *ApJS*, 24, 49  
 Reich, W., Fuerst, E., Reich, P., & Reif, K. 1990, *A&AS*, 85, 633  
 Reynolds, S. P. 1996, *ApJ*, 459, L13  
 Reynolds, S. P., & Keohane, J. W. 1999, *ApJ*, 525, 368  
 Sato, F. 1977, *PASJ*, 29, 75  
 Völk, H. J., Berezhko, E. G., & Ksenofontov, L. T. 2005, *A&A*, 433, 229  
 Ubertini et al. 2005, *astro-ph/0505191*  
 Uchiyama, Y., Aharonian, F. A., Takahashi, T., Hiraga, J. S., Moriguchi, Y., & Fukui, Y. 2005, *AIP Conf. Proc.* 745: High Energy Gamma-Ray Astronomy, 745, 305

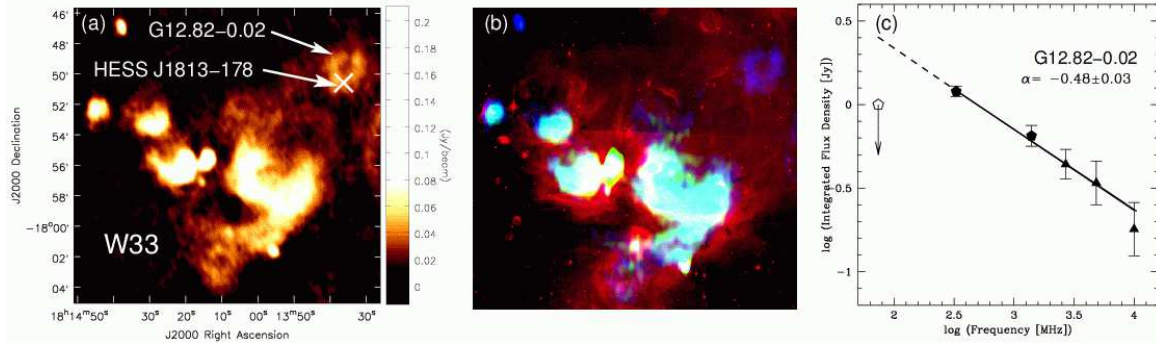


FIG. 1.— (a) VLA 90cm image of G12.82–0.02 with  $32'' \times 19''$  resolution. The cross indicates the position of HESS J1813–178 which has a positional uncertainty of  $1' - 2'$  (Aharonian et al. 2005b). (b) Three color image of the same region as (a), with red=*Spitzer* 8  $\mu\text{m}$ , green=VLA 20cm, and blue=VLA 90cm. Thermal emission is white to cyan or red in color, while non-thermal emission is darker blue. (c) Radio spectrum for SNR G12.8–0.0. Solid hexagon symbols are from the current work at 20 and 90cm. The open hexagon symbol indicates the  $5\sigma$  4m upper limit. The  $\blacktriangle$  symbols indicate flux densities from the 11cm Bonn, 6cm Parkes, and 3cm Nobeyama single dish surveys (Reich et al. 1990; Haynes et al. 1978; Handa et al. 1987). The line (solid and dashed) shows a power-law weighted least squares fit to the radio data for  $\nu \geq 330$  MHz (90cm).

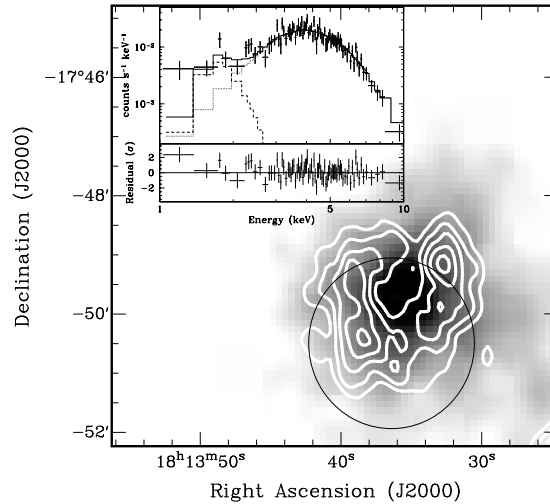


FIG. 2.— ASCA SIS greyscale image of AX J1813–178 in the energy range 0.5–10 keV smoothed to  $30''$  with 90cm contours from Fig. 1a at 28, 33, 38, 43, and 48  $\text{mJy beam}^{-1}$  overlaid (contour intervals are  $2\sigma$ ). The black circle indicates the position and angular extent ( $3'$ ) of HESS J1813–178. *Inset* ASCA SIS spectrum of AX J1813–178 extracted from  $3'$  region encompassing the radio shell. The cross symbols show the data while the solid line shows the best fit power-law (dotted line) plus RS (dashed) model. The residuals in the form of the uncertainty  $\sigma$  are shown in the bottom panel.

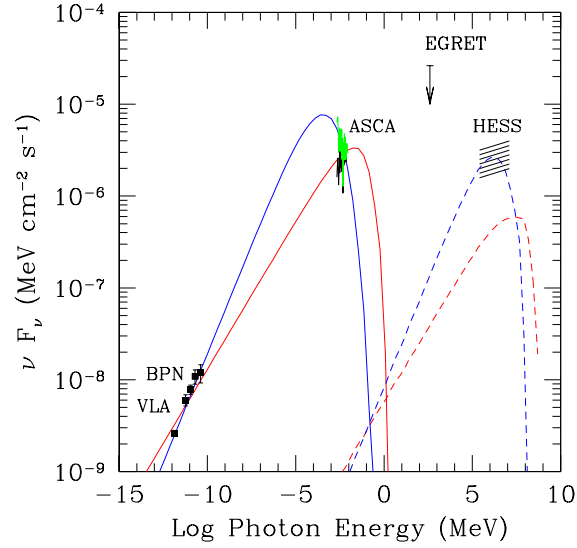


FIG. 3.— Fits to the broadband emission assuming that all the flux originates from the shell of SNR G12.8–0.0. BPN stands for Bonn, Parkes, and Nobeyama. The diagonal black lines indicate both the uncertainty in the HESS flux measurements, and the fact that no spectral information has yet been published for the TeV emission. The two models indicated by the red and blue lines show the range of parameter space that best fit the data: the *red* model uses the spectral index from the best fit to the ASCA data  $N_{\text{H}}$  of  $10.8 \times 10^{22} \text{ cm}^{-2}$  (black X-ray spectrum), while the *blue* model uses the spectral index implied by the  $1\sigma$  lower limit to  $N_{\text{H}}$  of  $8.9 \times 10^{22} \text{ cm}^{-2}$  (green X-ray spectrum). Both models include contributions from synchrotron (solid lines) and IC (dashed lines) mechanisms; we have assumed that the filling factor of the magnetic field in the IC emitting region is 15%.